Mechanics, Dynamics, and Control of a Single-Input Aquatic Vehicle With Variable Coefficient of Lift

Scott D. Kelly, *Member, IEEE*, and Ramadev B. Hukkeri

***Abstract*—We describe basic considerations in the Lagrangian modeling of aquatic vehicles developing liftlike forces in a controlled way. We introduce the aquatic Flettner rotor as prototypical of this class of vehicles, and demonstrate the compatibility of Lagrangian formalism with experimental data describing a laboratory rotor. We analyze the controllability of a model for the rotor, connect its structure to that of models for Lagrangian systems subject to nonholonomic constraints, and present numerical evidence that our model can behave chaotically given physically motivated inputs and disturbances. We conclude with a description of a fish-like robotic vehicle employing a rotor in place of a caudal fin.**

***Index Terms*—Fluid mechanics, Lagrangian systems, nonlinear control, robotic locomotion, underactuated systems.**

I. Introduction

A SOLID BODY moving through a fluid experiences surface forces which are absent in the absence of the fluid; a submerged body which controls its shape can exploit these forces to execute spatial trajectories unavailable to a free deforming body. A robotic vehicle moving through water on a macroscopic scale can experience hydrodynamic forces of at least three distinct kinds. *Inertial* forces, such as those reflected in classical notions like effective mass, are present in inviscid and viscous models alike [1]. Purely *viscous* forces, such as dominate problems in locomotion at low Reynolds number, account for drag through the dissipation of energy [2]. *Liftlike* forces, which play a central role in the locomotion of the most agile and efficient of fish, reflect the interplay of inertial and viscous phenomena [3].

Considered individually, inertial and viscous forces admit elegant, and quite parallel, descriptions in the language of geometric, particularly Lagrangian, mechanics [4]. Problems in robotic locomotion through fluids in which inertial or viscous forces are assumed, individually, to dominate are, therefore, accessible to recent geometric methods in nonlinear motion-planning and control, invoking notions like *geometric phase* [4]–[8]. While liftlike forces have been introduced *ad hoc* to otherwise geometric models for aquatic locomotion [9], in contrast, a Lagrangian formalism has yet to be obtained through which liftlike forces are realized from basic principles.

This omission is not simply the result of neglect. Fundamental differences between liftlike forces and inertial forces prevent the naive extension of the Lagrangian approach of [4] and [10] to flows which are not irrotational and acyclic. In particular, the total kinetic energy in a planar ideal flow with a circulatory component cannot be finite if the flow extends to infinity, even if the velocity of the fluid tends to zero at infinity. The significance of formal Euler–Lagrange equations with respect to a Lagrangian equal to the total kinetic energy is thus unclear in this case. We detail this issue in Section II, summarizing the state of the art in treating aquatic locomotion problems as problems in Lagrangian mechanics.

The issue of divergent kinetic energy arises in its simplest form in treating the problem of a circular cylinder translating through an infinite ideal fluid with nonzero circulation around the cylinder's boundary. It is this system that we explore in this paper, proposing a model in which the inertial effects of the fluid are incorporated into the Lagrangian, but the lift experienced by the cylinder is treated as a nonconservative external force. The Lagrangian, derived from the isolated acyclic component of the flow around the cylinder, converges as it does in [4] and [10]. We demonstrate the validity of this approach, at least to first order, with a simple robotic device comprising a vertical circular cylinder which is free to translate through a pool of water while driven to spin about its vertical axis of symmetry. We demonstrate in Section III that the behavior of this system is approximated by that of a model which regards the rotor as a body with a constant effective mass subject to a certain external force.

The dependence of lift on the translation and rotation of a circular cylinder in a transverse flow has been carefully characterized in the fluid dynamics literature under the assumption of steady flow [11]. Our experiments involve unsteady flows; we deduce the forces experienced by our device and compare the results with those predicted by the steady-flow model. It is not necessarily our goal to match a more complicated model to the dynamics of the physical system with higher fidelity; the experimental subtleties of characterizing the latter properly would exceed the scope of this paper. We validate the steady-flow model alongside a more complicated empirical model and, in part for reasons to be addressed below, adopt the simpler for subsequent analysis.

Following the conventional definition of lift, the liftlike force we consider in our simplified model is gyroscopic, in that it remains perpendicular to the instantaneous direction of motion of

Manuscript received January 6, 2005; revised November 23, 2005. This paper was recommended for publication by Associate Editor L. Whitcomb and Editor K. Lynch upon evaluation of the reviewers' comments. Color versions of Figs. 2, 3, 5–8, 11, and 12 are available online at http://ieeexplore.org.

S. D. Kelly is with the Department of Mechanical Science and Engineering, University of Illinois at Urbana-Champaign, Urbana, IL 61801-2906 USA (e-mail: sdk@uiuc.edu).

R. B. Hukkeri was with the Department of Mechanical and Industrial Engineering, University of Illinois at Urbana-Champaign, Urbana, IL 61801-2906 USA. He now resides in Chicago, IL 60625-5710 USA (e-mail: ramadev@gmail.com).

Digital Object Identifier 10.1109/TRO.2006.882934

the cylinder. We expect more complicated models for the dynamics of underwater vehicles to uphold the gyroscopic nature of the relevant liftlike forces. As control inputs, such forces lead to interesting controllability issues; we explore their relevance to our model in Section IV.

It is a basic property of gyroscopic forces that such forces do no work. This property is shared with forces of constraint in the context of nonholonomic mechanics. Indeed, a gyroscopic force can always be treated formally in terms of an equivalent (time-varying) constraint. We demonstrate in Section V that this is explicitly possible for our test system, forming a link to the geometric treatment of nonholonomic systems, and thus rendering the system accessible to elaborations of control methods like those advanced in [12]–[15].

The identification of the gyroscopic force on a lifting body with an equivalent constraint is not entirely artificial. The dynamics of a body developing liftlike forces are coupled to the dynamics of the surrounding fluid through vortex shedding. An essentially viscous phenomenon, vortex shedding can be modeled in an inviscid setting by introducing hydrodynamic constraints, Kutta conditions, which restrict, for example, the flow over a wing section with a sharp trailing point to stagnate at this point. In this sense, liftlike forces are derived from physical constraints.

Despite our simplified representation of lift as a function of translational and rotational speed, the addition of a constant external force to our model can give rise to surprisingly rich dynamics. We consider, in particular, the interplay of a sinusoidal control input with a force derived from a linear spatial potential in Section VI. The rectification of sinusoidal inputs is a fundamental paradigm in locomotion [5], and it is natural to consider the operation of an underwater vehicle in the presence of a force like that of gravity. To the authors' knowledge, the emergence of complex dynamics from the interaction of a periodic gyroscopic force and a spatial potential are explicitly documented for the first time here. We postpone for future work an exploration of the impact refinements to our lift model might have on the complexity of the system's dynamics.

Our investigation of robotic actuators which develop liftlike forces in water is driven, ultimately, by an interest in the mechanics of biomorphic aquatic locomotion. Detailed investigations of the hydrodynamics of fishlike swimming, such as that in [3] or [16], suggest a simplified view in which the caudal fin of a fish is regarded as a small lifting body which undulates behind the main body, the circulation around the fin oscillating with the position of the fin to generate liftlike thrust. If this description is valid, it should be possible to drive a fishlike body with a periodically spinning cylinder in place of an undulating fin. We describe a preliminary robotic system in Section VII which demonstrates this possibility.

II. Lagrangian Mechanics of Bodies in Fluids

In this section, we summarize inviscid aquatic locomotion as a problem in geometric mechanics, reconciling the abstract formalism with certain classical concepts and illuminating the sense in which the system examined in subsequent sections exceeds the scope of the existing literature. The approach we propose to broaden this scope has not been presented elsewhere.

The Lagrangian description of a mechanical system begins with a choice of *configuration manifold*, distinct points in which correspond to distinct arrangements of the material particles in the system. If we define a reference configuration for the set of material particles comprising a solid body surrounded by a fluid, any other configuration may be identified with a map from the region occupied by this system to itself.

Consider, for the sake of concreteness, the self-propulsion of a deformable planar body in an infinite fluid. The configuration manifold Q is defined in this case to comprise maps $\phi : \mathbb{R}^2 \to \mathbb{R}^2$ which restrict to diffeomorphisms $\phi_{B_0} : B_0 \to B$ and $\phi_{F_0} : F_0 \to F$ taking solid particles to solid particles and fluid particles to fluid particles, respectively. If we assume the fluid to be inviscid, we allow each ϕ to be discontinuous along the interface between body and fluid. If we assume the fluid to be incompressible, we require each restriction ϕ_{F_0} to be volume-preserving.

A Lagrangian is given for this system by the integral of the pointwise kinetic energy over all solid and fluid particles in the system. If the flow is irrotational and acyclic, this integral will converge, provided the fluid at infinity is stagnant. The total energy is invariant under free actions of two particular Lie groups on the configuration manifold Q. The *fluid particle relabeling group* $\mathrm{Diff}_{\mathrm{vol}}(F_0)$, comprising volume-preserving diffeomorphisms of the reference fluid region F_0 to itself, acts on Q on the right. The Euclidean group $\mathrm{SE}(2)$, comprising planar translations and rotations of the body accompanied by compatible deformations of the fluid, acts on Q on the left. Corresponding to each of these actions is a *momentum map*, the image of which will be conserved following Noether's theorem if, as will be the case if the fluid is inviscid, the system conserves energy [17].

The momentum map $\mathbb{J}_{\mathrm{Diff}_{\mathrm{vol}}(F_0)}$ takes its values in the vector space of spatial fluid vorticity fields paired with scalar circulations around the body [18]. If $u(x) = \dot{\phi} \circ \phi^{-1}(x)$ denotes the spatial fluid velocity field in terms of coordinates x on F, the vorticity can be thought of as the curl $\zeta(x) = \nabla \times u(x)$, and the circulation around an oriented spatial contour as the integral of the tangential component of $u(x)$ along that contour.

Restriction of the system's dynamics to the level set $\mathbb{J}_{\mathrm{Diff}_{\mathrm{vol}}(F_0)} = 0$ in the inviscid case is equivalent to the specification of potential flow outside the body. In this case, trajectories in Q for the fluid-body system are in one-to-one correspondence with trajectories in Q_{body}, the restriction of Q to the body, for a reduced Lagrangian system. Reduced systems of this kind are studied in detail in [4] and [10].

Note that Q_{body} is the Cartesian product $M \times \mathrm{SE}(2)$, where M is the shape manifold comprising body deformations, and $\mathrm{SE}(2)$ can now be thought to comprise rigid translations and rotations of the body alone in the plane. The momentum map $\mathbb{J}_{\mathrm{SE}(2)}$ takes its values in the space of Kelvin impulses and impulse couples [19], which serve as the body's equivalent linear and angular momenta as it moves through the fluid. If $\mathbb{J}_{\mathrm{SE}(2)}$ is conserved, restriction of the system's dynamics to the level set $\mathbb{J}_{\mathrm{SE}(2)} = 0$ provides further-reduced equations of motion in the form

$$T_g L_{g^{-1}} \dot{g} + A(r)\dot{r} = 0 \tag{1}$$

where $r(t) \in M$ denotes the body's shape, $g(t) \in \mathrm{SE}(2)$ denotes the body's position and orientation with respect to a stationary frame, and the *local principal connection form* $A : TM \to \mathfrak{se}(2)$ encapsulates everything about (1) that is not generic to driftless planar locomotion problems [5].

Because it relies on the assumption of an ideal fluid, the model (1) describes a system in which inviscid forces are present, but liftlike forces are not. In particular, the Kutta–Joukouski theorem asserts that the lift developed on a planar body translating with velocity $\mathbf{v}$ through a fluid with density ρ is given, as a vector quantity, by

$$\mathbf{L} = -\rho \mathbf{v} \times \mathbf{\Gamma} \tag{2}$$

where the vector $\mathbf{\Gamma}$ has magnitude equal to the circulation around the body, and is directed out of the plane according to the right-hand rule [20], [21]. Since (1) assumes $\mathbb{J}_{\mathrm{Diff_{vol}}(F_0)} = 0$, and thus $\Gamma = 0$, the body experiences no lift.

There exists, nevertheless, a well-developed classical theory of planar lifting bodies. Joukowski airfoil theory [22] augments the requirement that the flow around the cross-sectional contour of a wing be derived from a potential function, with the requirement that the flow stagnate at the contour's (typically sharp) trailing point. If the contour is moving relative to the fluid infinitely far away, this boundary condition generically introduces a circulatory component to the flow around the contour, thus providing lift. Such boundary conditions are called Kutta conditions.

In general, constraints are introduced to a Lagrangian system as restrictions among the velocities corresponding to generalized coordinates on the configuration manifold Q. Velocity constraints which can be integrated with respect to time to provide direct constraints on Q are said to be *holonomic*, while constraints which cannot are said to be *nonholonomic*. The requirement that the planar flow over a wing section should stagnate at a certain point is the requirement that a certain pair of adjacent solid and fluid particles should remain adjacent; this is evidently a holonomic constraint on the planar system. Consider, in contrast, the flow over a *finite* wing. Such a flow may be consistent with traditional Kutta conditions in all cross-sections of the wing, yet no direct restriction need be placed on the location of individual fluid particles if the flow can attach and detach transverse to these sections at the endpoints of the wing's trailing edge. We propose that the nonholonomic constraint enforcing planar Kutta conditions along a hydrofoil while permitting transverse flow be considered a more general *Kutta constraint*. Note that Kutta conditions for unsteady flows have been described elsewhere [23].

The passage from existing ideal flow models for aquatic locomotion to models which accommodate vortex shedding for propulsion requires, in the language of Lagrangian mechanics, the determination of models specifying the coupling between evolution equations for momentum maps like $\mathbb{J}_{\mathrm{SE}(2)}$ and $\mathbb{J}_{\mathrm{Diff_{vol}}(F_0)}$ above. In Section V, we show that the equation of motion for our spinning cylinder can be written in the form

$$T_g L_{g^{-1}} \dot{g} + A_{\mathrm{nhc}}(r)\dot{r} = \Upsilon(r)p \tag{3}$$

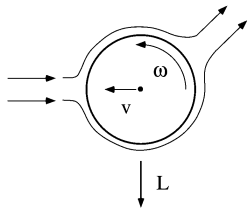

Fig. 1. Cross-section of a Flettner rotor.

where $A_{\mathrm{nhc}}(r) : TM \to \mathfrak{se}(2)$ represents a *nonholonomic connection* in the sense of [24], and the conserved quantity related to body motion is not $\mathbb{J}_{\mathrm{SE}(2)}$ but a related *nonholonomic momentum* $p \in \mathfrak{se}(2)^*$. This equation encodes the variation in $\mathbb{J}_{\mathrm{SE}(2)}$ over time as a result of the liftlike force on the cylinder. The analogous equation describing the evolution of $\mathbb{J}_{\mathrm{Diff_{vol}}(F_0)}$ will be developed in another paper. Note the difference between (1) and (3).

III. Submerged Robotic Flettner Rotor

A. Circulation and Energy Divergence

Fig. 1 depicts the simplest possible abstraction of the planar hydrofoil, a cylinder with rigid circular cross-section. It is well known that a circular cylinder which rotates about its longitudinal axis while translating through air or water will experience a lift force perpendicular to its translational velocity. This phenomenon parallels that inducing a spinning tennis ball or baseball to curve in flight. If we assume the spinning of the cylinder to introduce a circulatory component to the surrounding flow, this phenomenon, known alternately as the Magnus effect or the Robins–Euler effect, is precisely in line with (2). The magnitude of the lift developed on a translating airfoil of rigid noncircular profile is often practically related to the foil's shape and speed with a scalar coefficient of lift [22]; variations in the angular velocity ω vary the effective coefficient of lift of the cylinder in Fig. 1.

We refer to a circular cylinder which rotates about its longitudinal axis to generate lift as a *Flettner rotor*. Anton Flettner constructed sailing ships and windmills with rotating cylinders in place of airfoils in the 1920s [20], [25]. The Cousteau Society presently operates two vessels with similar "turbosails," and the Flettner-rotor paradigm has recently been revisited in the context of ship design for the deployment of spray turbines [26].

In proceeding from the Lagrangian treatment of locomotion in acyclic flow [4], [10], it would seem natural to pursue a model for the system depicted in Fig. 1 by assuming the rotation of the cylinder to determine a circulation with the same orientation, to add a circulatory flow depending on ω to the flow induced by the translation of the cylinder, and to define a Lagrangian from the total kinetic energy in the system. The difficulty arises in the fact that the kinetic energy diverges for any infinite circulatory flow in the plane. The fluid velocity field around a circular cylinder with radius R translating with velocity $\mathbf{v}$ through an ideal fluid is given, in particular, in polar coordinates centered in the cylinder, by

$$u_r = |\mathbf{v}|\frac{R^2}{r^2}\cos\theta, \quad u_\theta = |\mathbf{v}|\frac{R^2}{r^2}\sin\theta + \frac{\Gamma}{2\pi r}.$$

Although u_r and u_θ both vanish as r tends to infinity, the integral of $(1/2)\rho(u_r^2+u_\theta^2)$ over the fluid is infinite. Indeed, this problem persists in three dimensions if the flow around any cross-section of a solid body is assumed to be circulatory, even if fluid is allowed to flow perpendicular to this section to ameliorate rotational contributions to the system's total energy.

We do not, however, despair that the dynamics of a planar body developing lift possess a meaningful Lagrangian description. As a starting point, we note that the infinite kinetic energy of the circulatory flow around a planar body is that of the flow around a single point vortex, in the sense that the flow around the body approaches the flow around a vortex as the distance from the body increases. This is the origin of the *substitution vortex* concept [1]. The equations of motion for a system of point vortices in a planar inviscid fluid have long been known to possess a Hamiltonian structure, regardless of the strengths of the individual vortices [27], [28].

An infinite planar fluid admits an unreduced Hamiltonian treatment dual to the unreduced Lagrangian treatment described in Section II with the body removed. The total energy in the system provides the Hamiltonian function; this energy will converge if the fluid is irrotational. The total energy will *not* converge if the spatial fluid velocity field contains a system of point vortices with strengths that do not sum to zero, yet it can be shown that the formal process of Hamiltonian reduction yields the correct equations governing the evolution of any system of point vortices [18]. The reduced Hamiltonian structure in this problem was recognized a century before the link was made to the unreduced structure.

Inspired by the problem of point vortices in the plane, we proceed in the remainder of this section to develop a simple model for the dynamics of a free circular cylinder developing lift from basic considerations and empirical data. The Lagrangian structure in this model is identified after the fact. We do not endeavor here to link this model, a reduced equation in the sense of Section II, to the unreduced equations for a body coupled to an infinite fluid, but we note that the Hamiltonian structure inherent to the interaction of a free cylinder with a system of point vortices was illuminated by one of the authors and colleagues in [29].

B. Experimental Apparatus

Fig. 2 depicts an experimental Flettner rotor. A smooth Lucite rod 1.9 cm in diameter protrudes 25 cm downward from a styrofoam ring, the latter buoyant in an 8-ft pool of water. Flettner himself focused on rotors in air; ours is a submerged robotic Flettner rotor, or SuRFR. A DC motor mounted above the ring drives the rod to spin about its vertical axis of symmetry. We note that the ring itself rotates very little during experimental tests of this system in the pool.

It is our goal to develop and validate a model for the development of lift on the SuRFR as a viscous phenomenon distinct from the development of drag, yet our laboratory system is innately subject to drag. Fig. 3 depicts an apparatus to compensate for this drag. A horizontal fan pivots freely atop the SuRFR, coupled to a small fin submerged outside the foam ring. When the rotor has no angular velocity, this fan imparts a forward thrust to balance the drag on the rotor, and the SuRFR moves in a straight line at constant speed. This behavior simulates that of a cylinder given a nonzero initial velocity in an ideal fluid. When the spinning of the rotor imparts a lateral liftlike force to the moving SuRFR, inducing it to turn, the fin situates itself directly behind the SuRFR along its instantaneous direction of motion, and the fan maintains translational speed. We will revisit the constancy of this speed, consistent with the model described in Section III-C, in Section IV.

Fig. 2. Experimental SuRFR.

Fig. 3. Fan for passive drag cancellation.

Motor control and data acquisition are coordinated with MATLAB and WinCon software running on a PC with a Texas Instruments 6711 DSP board and a custom-built motor control

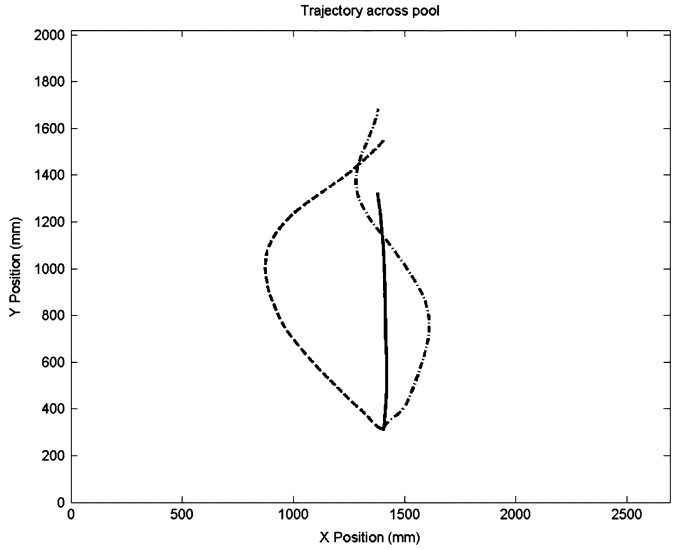

Fig. 4. Experimental SuRFR trajectories.

daughterboard. The SuRFR is tethered to the daughterboard and a power supply, but the tether is suspended from above to induce minimal drag on the SuRFR as it translates in the pool. We measure position data using a ceiling-mounted Logitech Quickcam Pro 4000 USB camera sampling at 15 frames per second; the top of the SuRFR is painted black to contrast the light blue pool floor.

Fig. 4 depicts three trajectories executed by the SuRFR, each beginning at the same point in the plane and approaching the same target region. The straight trajectory is unactuated; the remaining trajectories reflect different oscillatory variations in the rotor speed ω. The SuRFR can also execute looped trajectories if ω is held constant. We focus our attention on periodic trajectories with nonzero mean translational components, in keeping with our analogy between the SuRFR and a lifting body like the caudal fin propelling a carangiform fish [3], [9], [30]. We will revisit the SuRFR as an abstraction of the carangiform caudal fin in Section VII.

We note that each of the trajectories depicted in Fig. 4 can be reproduced experimentally at any translational speed, the translational speed determining the necessary variations in the rotor speed over time. This will become clearer when we discuss modeling below.

C. A Priori Modeling

If (x, y) denotes the horizontal position of the center of the SuRFR with respect to a laboratory frame, m denotes the SuRFR's effective mass, and we assume $\dot{\Gamma}$, the rate at which the circulation around the rotor changes, to be controlled directly, idealized equations of motion for the SuRFR can be written, following (2), as the control-affine nonlinear system with drift

$$\frac{d}{dt}\begin{bmatrix} x \\ v_x \\ y \\ v_y \\ \Gamma \end{bmatrix} = \begin{bmatrix} v_x \\ -(\rho\Gamma/m)v_y \\ v_y \\ (\rho\Gamma/m)v_x \\ 0 \end{bmatrix} + \begin{bmatrix} 0 \\ 0 \\ 0 \\ 0 \\ 1 \end{bmatrix}\tau. \tag{4}$$

Here v_x and v_y denote the components of the translational velocity $\mathbf{v}$ in the x and y directions, respectively, and τ denotes the single control input. Given a periodic input $\tau(t)$, the SuRFR will, according to this model, execute trajectories like those shown in Fig. 4 if its translational speed is nonzero. In reality, we exert control influence directly on ω, not Γ. The assumption that these are related linearly, so that $\dot{\Gamma}$ can be treated as an abstract input, follows from the definition of Γ given the no-slip condition generally enforced in the study of viscous flows on solid boundaries [1], [31].

The lift on a circular cylinder rotating about its longitudinal axis in a steady, nonzero transverse flow has been investigated experimentally several times since Magnus [32]. It has been demonstrated, in particular, that this lift varies roughly linearly with the rotational speed $|\omega|$ and quadratically with the relative flowspeed $|\mathbf{v}|$ in the Reynolds number range $10^3 < \mathrm{Re} < 10^4$ [11]. The experiments depicted in Fig. 4 represent Reynolds numbers within this range. A reduced Lagrangian model which averts the difficulty with infinite energy described earlier, but which relies on an empirical expression for lift as a function of linear and angular velocity, may be obtained by treating the lift on the SuRFR as an external force imposed on an inviscid Lagrangian system. The dynamics of the SuRFR may be regarded, in particular, as those of a solid body with a certain *effective mass* [33] subject to a force dependent upon its translation and rotation. The effective mass we observe for the SuRFR accounts, in practice, for both the mass of the device itself and the added-mass effects of the water on the cylinder and support ring.

If we define the Lagrangian

$$L = \frac{1}{2}m_{\text{effective}}(\dot{x}^2 + \dot{y}^2) \tag{5}$$

and, following [11], consider the cylinder to move according to Euler–Lagrange equations subject to the force field

$$\mathbf{L} = k\omega\sqrt{\dot{x}^2 + \dot{y}^2}\begin{bmatrix} -\dot{y} \\ \dot{x} \end{bmatrix} \tag{6}$$

our final model takes the form

$$m_{\text{effective}}\begin{bmatrix} \ddot{x} \\ \ddot{y} \end{bmatrix} = k\omega\sqrt{\dot{x}^2 + \dot{y}^2}\begin{bmatrix} -\dot{y} \\ \dot{x} \end{bmatrix} \tag{7}$$

where k is a constant to be determined empirically.

D. Model Validation

Before analyzing the model (7) in the sections to come, we verify it against the observed behavior of the device in Figs. 2 and 3. The design of the SuRFR does not allow for the direct measurement of the liftlike forces it experiences; we therefore endeavor to infer these forces from a large body of trajectory data like that presented in Fig. 4.

Our approach is to track the SuRFR as it executes a variety of maneuvers corresponding to known time variations in ω and to infer the time-varying lift from the geometry of each trajectory. This is a coarse method, relying on the assumption that the net

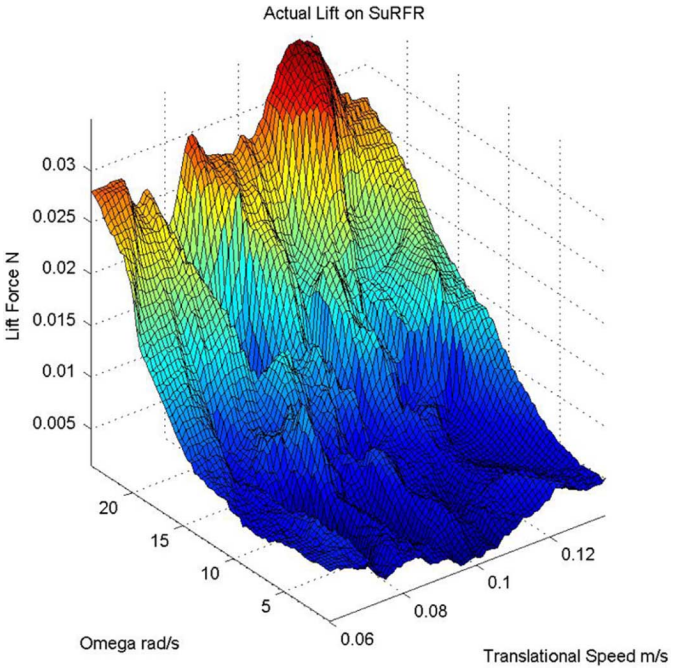

Fig. 5. Lift computed from trajectory data.

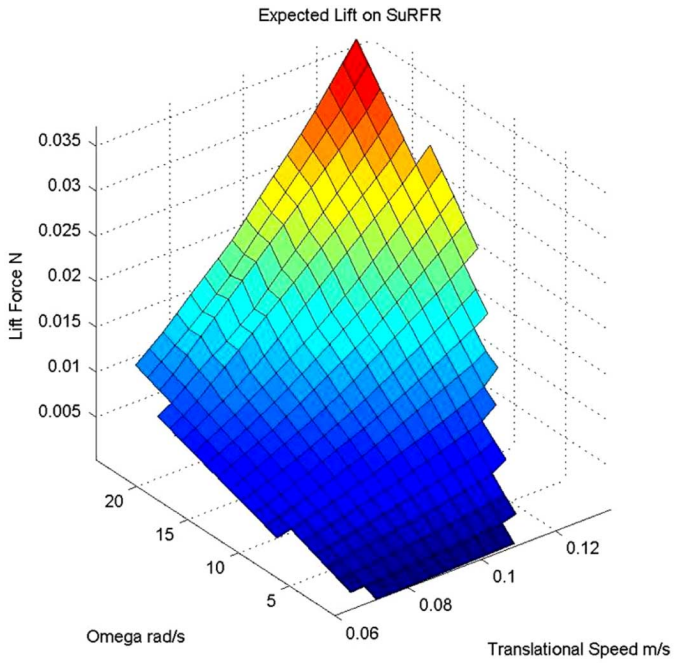

Fig. 6. Lift predicted by (6).

force experienced by the SuRFR remains exactly perpendicular to its observed instantaneous velocity. Since the water in the pool is excited by the motion of the SuRFR, the velocity of the SuRFR relative to nearby water may differ in a time-varying way from its velocity relative to the camera used to collect data, coloring the data in a manner that would be difficult to isolate. We note, however, that observed disturbances to the surface of the water during data collection are minimal.

Fig. 5 depicts the magnitude $|\mathbf{L}|$ computed from our trajectory data in the manner described above as a function of $|\omega|$ and $|\mathbf{v}|$. The raw data are noisy, as predicted, but indicate some clear trends. The data shown correspond to Reynolds numbers in the lower one-fourth of the range $10^3 < \mathrm{Re} < 10^4$ cited for the validity of (6) in the steady-flow case.

Fig. 6 depicts the surface corresponding to that in Fig. 5 as predicted by (6) with $k = 0.10$. It is apparent that the model provides an approximate fit to the experimental data for the higher translational speeds shown, and for all translational speeds when the rotor speed is low, but substantially underestimates the lift observed for lower translational speeds when the rotor speed is high. This may be attributable to the variation of the Reynolds number away from the center of the range cited above, but may also result from increased error in our experimental method when the rotor spins quickly but translates slowly. The effects of rotor imbalance are amplified under these circumstances, for example, as are the aforementioned effects of disturbances by the rotor to the surrounding fluid, which the model assumes to be quiescent. We note that with the choice $k = 0.10$, the effective mass of the SuRFR is computed to be 1.1 kg. The actual mass of the device is 0.89 kg.

We note that a better fit to the data in Fig. 5 can be obtained with a model of the form

$$|\mathbf{L}| = \max(k|\omega|^a|\mathbf{v}|^b - c, d) \tag{8}$$

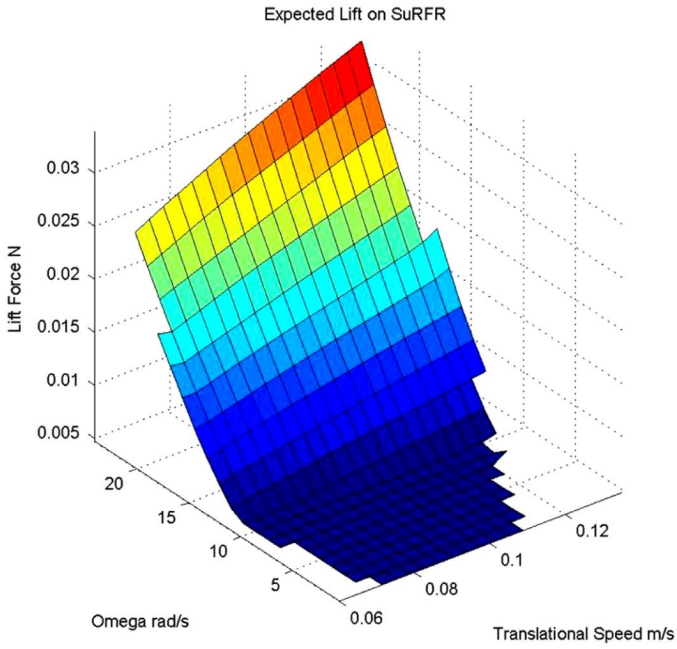

Fig. 7. Lift predicted by (8).

such as is depicted in Fig. 7 for the case $(k, a, b, c, d) = (0.00040, 1.8, 0.48, 0.0036, 0.0047)$. We have not sought careful physical explanations for our most successful empirical models of this form.

IV. Local and Global Controllability

A. Controllability Without an External Load

It is straightforward to show that the involutive closure of the drift and control vector fields from (4) under the Jacobi–Lie bracket on $\mathbb{R}^5$ fails to be full-rank, so the system (4) fails the Lie algebra rank condition for local accessibility [34]. Indeed,

it is apparent from (4) that a rotor with zero initial translational velocity will be unable to generate motion by varying Γ, since the lift developed on the cylinder contains translational velocity as a multiplicative factor. Given any nonzero initial velocity, however, it is apparent from experiments that the SuRFR can reach any point in the plane from the origin by describing an appropriate sequence of arcs.

For clarity's sake, we now adopt the normalized model

$$\begin{bmatrix} \ddot{x} \\ \ddot{y} \end{bmatrix} = \omega\sqrt{\dot{x}^2+\dot{y}^2}\begin{bmatrix} -\dot{y} \\ \dot{x} \end{bmatrix}. \tag{9}$$

Since the lift is always perpendicular to the SuRFR's instantaneous velocity

$$\begin{aligned}\frac{d}{dt}(\dot{x}^2+\dot{y}^2) &= 2\dot{x}\ddot{x}+2\dot{y}\ddot{y} \\ &= 2\omega\sqrt{\dot{x}^2+\dot{y}^2}(-\dot{x}\dot{y}+\dot{y}\dot{x}) = 0\end{aligned}$$

and variations in ω cannot, in fact, change the SuRFR's translational speed. The lift $\mathbf{L}$ does no work and the Lagrangian (5) is conserved; the analogy to mechanical constraint forces which do no work is revisited in Section V. We may define the cylinder's instantaneous heading angle θ such that

$$\tan\theta = \frac{\dot{y}}{\dot{x}}. \tag{10}$$

It follows that $\dot{\theta}$ is proportional to ω. A torque input to the SuRFR thus controls, through two integrations, the direction of motion. We note, furthermore, that the instantaneous curvature

$$\kappa = \sqrt{\ddot{x}^2+\ddot{y}^2} \tag{11}$$

of a path described by the SuRFR is proportional to ω [35].

The fact that two arbitrary points in the plane can be joined by a differentiable curve with arbitrary initial and final velocities is proved in [36]. The problem considered in [36] is, in fact, that of finding the curve of minimum length satisfying specified end conditions, yet subject to a lower bound on the curvature κ. The SuRFR provides a mechanical realization of this problem. In practice, the curvature of a path described by the SuRFR is bounded below, due to physical considerations of motor speed and flow separation.

We note that it is tempting to specify the limitation on the curvature in this problem by requiring the radius of curvature to remain greater than or equal to some fixed value. The restriction considered in [36] is, instead, provided by the Lipschitz condition

$$\sqrt{(\dot{x}(t_1)-\dot{x}(t_2))^2+(\dot{y}(t_1)-\dot{y}(t_2))^2} \leq K^{-1}|t_1-t_2|$$

on the *average curvature* of the path described between any two points t_1 and t_2 in time. Here K is a positive constant. Differentiable trajectories of minimal length satisfying this condition comprise circular arcs and straight lines concatenated at points of tangency. It is clear that the curvature (11) is not defined where a straight arc and a circular arc are joined in this manner.

B. The Addition of an External Potential

We have noted our interest in the SuRFR as the prototypical aquatic vehicle exploiting liftlike forces for control. Real aquatic vehicles are subject to varied disturbances as they execute maneuvers; the force of gravity exemplifies a ubiquitous external force. The addition of a time-invariant external spatial force field to (9) leads to the equations

$$\begin{bmatrix} \ddot{x} \\ \ddot{y} \end{bmatrix} = \omega\sqrt{\dot{x}^2+\dot{y}^2}\begin{bmatrix} -\dot{y} \\ \dot{x} \end{bmatrix} + \begin{bmatrix} f(x,y) \\ g(x,y) \end{bmatrix}. \tag{12}$$

If this force is, like that of gravity, the spatial gradient of a potential function $F(x,y)$, then

$$\begin{aligned}\frac{d}{dt}(\dot{x}^2+\dot{y}^2) &= 2\dot{x}f(x,y)+2\dot{y}g(x,y) \\ &= 2\left(\dot{x}\frac{\partial F}{\partial x}+\dot{y}\frac{\partial F}{\partial y}\right) = 2\dot{F}\end{aligned}$$

where F is understood to depend on t through variations in the position (x,y). It follows that

$$|\mathbf{v}(t)|^2 = 2(F(t)-F(0))+|\mathbf{v}(0)|^2$$

meaning that the SuRFR cannot attain a nonzero velocity on the level set of points (x,y) satisfying

$$F(x,y) = F(x(0),y(0)) - \frac{1}{2}((\dot{x}(0))^2+(\dot{y}(0))^2). \tag{13}$$

This level set, if it exists, will separate reachable points from unreachable points. We revisit this issue in Section VI.

We have observed the SuRFR's inability to swim arbitrarily uphill, in the sense that its initial kinetic energy can be converted to potential energy, but its total energy cannot be increased through control. We distinguish swimming uphill from swimming upstream, the latter referring to motion with respect to the (potentially moving) frame of reference of the ambient fluid.

V. Nonholonomic Mechanics

Equation (1) relates changes in the shape of a solid body in an ideal fluid to the resulting motion of that body relative to a spatial frame. The local connection form $A : TM \rightarrow \mathfrak{se}(2)$ encodes this relationship, its range the Lie algebra corresponding to a symmetry group from which the system derives a conservation law. The introduction of nonholonomic constraints to a Lagrangian system can disrupt the system's adherence to laws like the conservation of linear or angular momentum, yet, because the corresponding forces of constraint do no work, need not disrupt the system's conservation of energy. The constraints can be understood to redirect momentumlike quantities, the magnitudes of which may be conserved.

This concept is made rigorous in [24], [37], and [38] with the definition of the *nonholonomic connection form*, which, in the context of planar locomotion, takes values in a time-varying subspace of $\mathfrak{se}(2)$. The nonholonomic connection is derived from a *nonholonomic momentum map*, just as the principal connection in (1) is derived from the conventional momentum map $\mathbb{J}_{\mathrm{SE}(2)}$. We sketch this construction here as it adapts to the SuRFR; we refer the reader to [24] for details.

The key, for our purposes, is to regard the heading angle θ from (10) as an additional effective configuration variable. If α denotes the rotation angle of the rotor, so that $\dot{\alpha} = \omega = \dot{\theta}/C$ for some positive constant C, we take the configuration manifold Q to be $\mathbb{S}^1 \times \mathrm{SE}(2)$ with coordinates $q = (\alpha, x, y, \theta)$.

We proceed, following [24], to define the distributions

$$D_q = \mathrm{span}\left\{\frac{\partial}{\partial\alpha} + C\frac{\partial}{\partial\theta}, \cos\theta\frac{\partial}{\partial x} + \sin\theta\frac{\partial}{\partial y}\right\} \subset T_qQ$$

$$S_q = \mathrm{span}\left\{\cos\theta\frac{\partial}{\partial x} + \sin\theta\frac{\partial}{\partial y}\right\} = D_q \cap T_q\mathrm{Orb}(q)$$

where $\mathrm{Orb}(q)$ is the orbit of the point $q = (\alpha, x, y, \theta)$ under left translation on $\mathrm{SE}(2)$ and consequently

$$T_q\mathrm{Orb}(q) = \mathrm{span}\left\{\frac{\partial}{\partial x}, \frac{\partial}{\partial y}, \frac{\partial}{\partial\theta}\right\}.$$

The distribution D_q, analogous in form to the constraint distribution defining a traditional nonholonomic system, encodes the relationships among velocities in the coordinates on Q imposed by the definition of θ.

We next define, for each $q \in Q$, the vector subspace

$$\mathfrak{g}^q = \{\xi \in \mathfrak{g} | \xi_Q(q) \in S_q\}$$

of $\mathfrak{g} = \mathfrak{se}(2)$ and the bundle $\mathfrak{g}^D$ over Q whose fiber at each $q \in Q$ equals $\mathfrak{g}^q$. The general theory developed in [24] calls for a choice of section ξ^q from $\mathfrak{g}^D$; the only logical choice for the SuRFR makes this section

$$\xi^q = (\cos\theta, \sin\theta, 0) \in \mathfrak{g}^q$$

at each q. The nonholonomic momentum map

$$\mathbb{J}^{\mathrm{nhc}} : TQ \to (\mathfrak{g}^D)^* : (q, \dot{q}) \mapsto m_{\mathrm{eff}}(\dot{x}, \dot{y}, 0)$$

is defined by the equality

$$\langle \mathbb{J}^{\mathrm{nhc}}(q, \dot{q}), \xi^q \rangle = \left\langle \mathbb{F}L(q, \dot{q}), \xi^q_Q \right\rangle$$

and the nonholonomic body momentum is given by

$$p = \langle \mathbb{J}^{\mathrm{nhc}}(q, \dot{q}), \xi^q \rangle = m_{\mathrm{eff}}(\dot{x}\cos\theta + \dot{y}\sin\theta).$$

Identifying $\mathfrak{g}^q$ with $T_{\xi^q}\mathfrak{g}^q$, we may write the equations of motion for the SuRFR in matrix form as

$$\begin{bmatrix} \dot{x}\cos\theta + \dot{y}\sin\theta \\ \dot{y}\cos\theta - \dot{x}\sin\theta \\ \dot{\theta} \end{bmatrix} + \begin{bmatrix} 0 \\ 0 \\ -C \end{bmatrix} \dot{\alpha} = \begin{bmatrix} \frac{1}{m_{\mathrm{eff}}} \\ 0 \\ 0 \end{bmatrix} p$$

which has the form (3), together with the scalar *momentum equation*

$$\dot{p} = \langle \mathbb{F}L(q, \dot{q}), (\dot{\xi}^q)_Q \rangle = m_{\mathrm{eff}}(-\dot{x}\sin\theta + \dot{y}\cos\theta)\dot{\theta} = 0. \quad (14)$$

VI. Periodic Inputs and Chaotic Trajectories

We return now to the response of the SuRFR to periodic inputs, this time in the presence of an external force of the form considered in Section IV-B. Subject to the simplest such nonzero force, derived from the linear potential $F(x, y) = x$ and thus aligned with a spatial coordinate axis, the normalized equations of motion for the periodically driven SuRFR take the form

$$\begin{bmatrix} \ddot{x} \\ \ddot{y} \end{bmatrix} = \sqrt{\dot{x}^2 + \dot{y}^2} \begin{bmatrix} -\dot{y} \\ \dot{x} \end{bmatrix} \sin\nu t + \begin{bmatrix} 1 \\ 0 \end{bmatrix}. \quad (15)$$

Despite the simplicity of this system, its behavior varies dramatically with the forcing frequency ν. Our objective in this section is to document this behavior; we plan a more thorough examination of the interplay of time-varying gyroscopic forces and spatially fixed potential forces in a future paper.

Fig. 8 depicts trajectories executed by this system for three different values of ν. In each case, the SuRFR begins at the origin with unit velocity in the x direction. We note that the set of points in the plane for which $F(x, y) = x = -1/2$ constitutes a separatrix according to (13); the SuRFR crosses this line in none of the three trajectory plots. We observe that the approximate periodicity in the trajectory corresponding to the case $\nu = 4.00$ is lost as ν is decreased.

Fig. 9 depicts Poincaré surfaces of section corresponding to different values of ν. In each case, the velocity

$$(v_x(2n\pi/\nu), v_y(2n\pi/\nu))$$

is plotted in the (v_x, v_y) plane for several thousand consecutive integer values of n. The scale of the images decreases with ν; the shape described by the surface of section when $\nu = 4.00$ forms the lower half of the shape described when $\nu = 2.00$, which in turn becomes the center of the spiral formed when $\nu = 1.00$. We assess the chaotic nature of the dynamics depicted in Fig. 8(c) by computing the *correlation dimension* of the surface of the section in Fig. 9(l), following a method introduced in [39].

The correlation dimension D_c of a set of points in the plane provides an estimate of, and a lower bound for, the Hausdorff dimension of that set. Given a small, positive real number ς, we define

$$C(\varsigma) = \frac{1}{N^2}(\text{number of pairs of points less than } \varsigma \text{ apart})$$

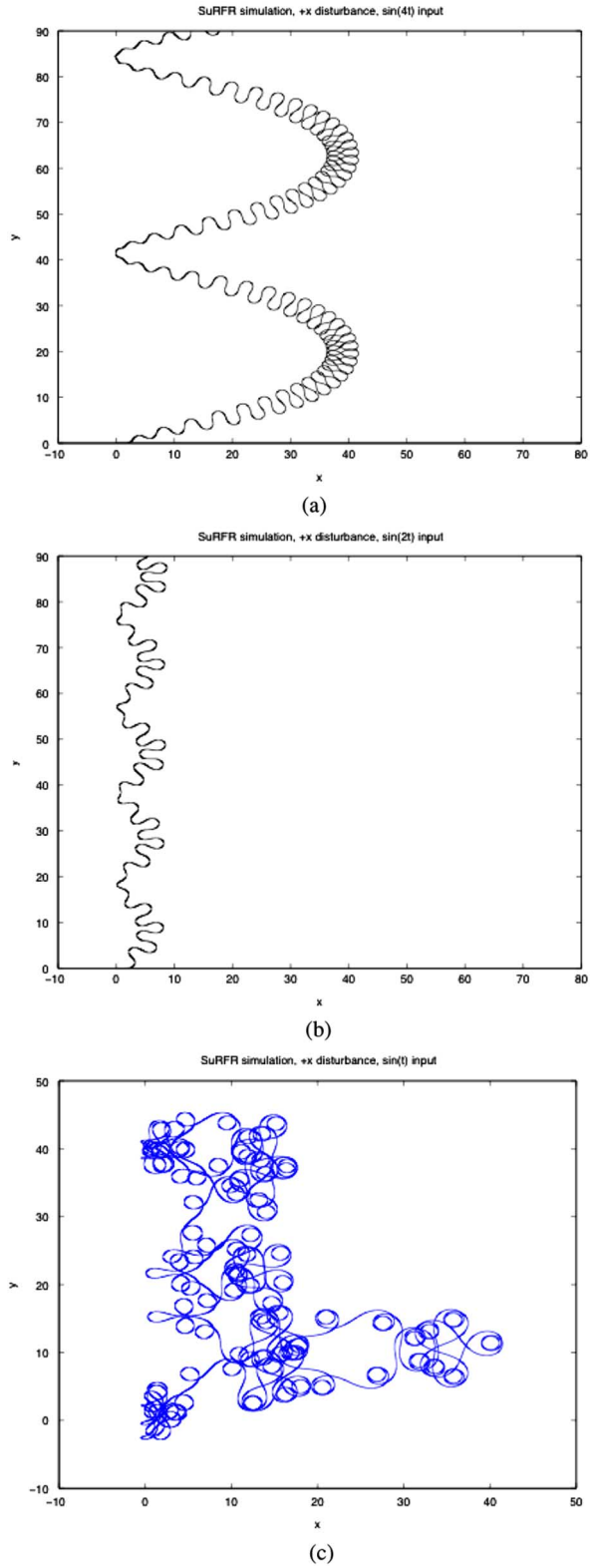

Fig. 8. Trajectories in (x, y) space. (a) $\nu = 4.00$. (b) $\nu = 2.00$. (c) $\nu = 1.00$.

where N is the total number of points considered. As a function of ς, this quantity will vary as $C(\varsigma) \sim \varsigma^{D_c}$. For the surface of section depicted in Fig. 9(l), we determine the correlation dimension in this way to be $D_c \approx 1.76$.

The Hausdorff dimension of the surface of section in Fig. 9(l) provides a measure of the deviation of the system's trajectory

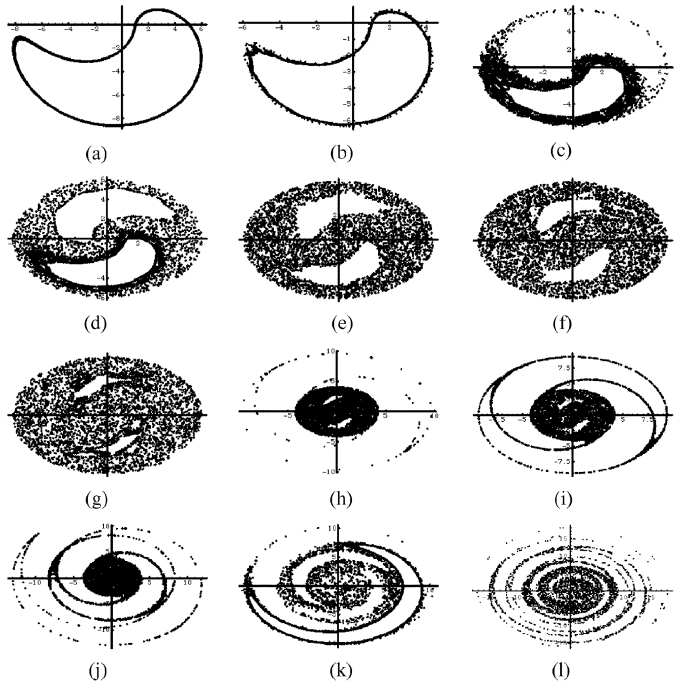

Fig. 9. Poincaré sections in (v_x, v_y) space. (a) $\nu = 4.00$. (b) $\nu = 3.00$. (c) $\nu = 2.70$. (d) $\nu = 2.50$. (e) $\nu = 2.00$. (f) $\nu = 1.90$. (g) $\nu = 1.80$. (h) $\nu = 1.75$. (i) $\nu = 1.70$. (j) $\nu = 1.50$. (k) $\nu = 1.20$. (l) $\nu = 1.00$.

in the (v_x, v_y) plane from periodic. If this trajectory were periodic, its dimension would be unity. Were it periodic with a frequency commensurate with ν, sampling points with frequency ν as shown would result in a surface of section with dimension zero. Were it periodic with a frequency incommensurate with ν, the surface of section could describe a set of points with dimension one, but no more. The higher fractal dimension of the surface of section in Fig. 9(l) indicates chaotic behavior.

As a final note, we observe that the forced system (15) is Hamiltonian with respect to the time-periodic function

$$H = -\frac{1}{3}\sqrt{\left(v_x^2 + v_y^2\right)^3}\sin \nu t + v_y.$$

The chaotic behavior of time-varying Hamiltonian systems is discussed in [40].

VII. Planar Propulsion With an Undulating Rotor

The locomotion of certain fish is characterized by the undulation of a caudal fin behind a body which remains, on the scale of this undulation, nearly undeformed. A planar model for carangiform locomotion of this sort is examined in [9]; it is demonstrated therein that propulsion can be achieved by the proper phasing of oscillations in the position of the fin behind the body and oscillations in the circulation about this fin.

Figs. 10 and 11 depict a robotic device which models carangiform locomotion with a rotating cylinder in place of a caudal fin. The position of the cylinder with respect to the body and the speed at which the cylinder rotates are controlled independently. It is anticipated that this device will illuminate the phasing of fin position and circulation in the swimming of fish; it also provides a prototype for more sophisticated aquatic robots using Flettner

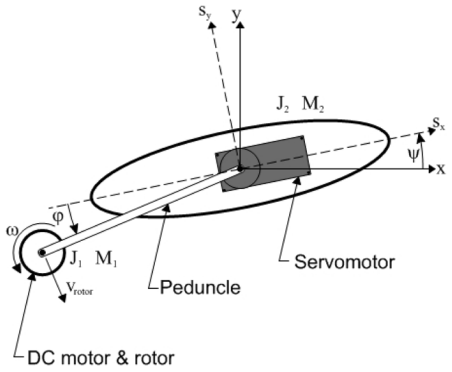

Fig. 10. Flettner rotor in place of a caudal fin.

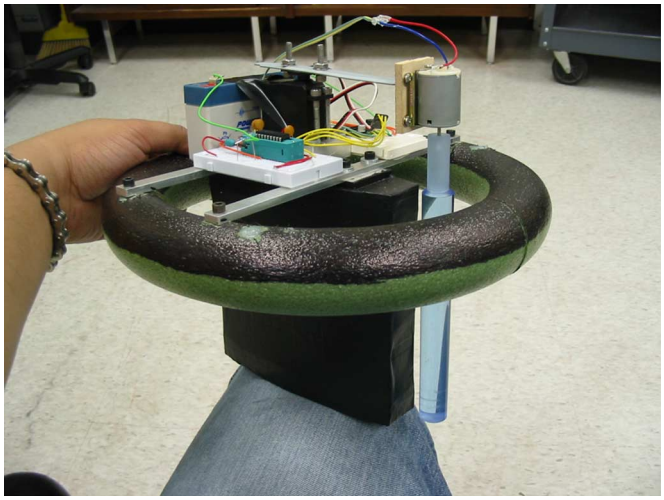

Fig. 11. Prototypical carangiform robot.

rotors as appendages for propulsion and steering. We note, in particular, that the swimming of carangiform fish has attracted attention because of its energy efficiency, and is associated with a distinctive wake pattern [3], [41]. Since variations in the position of the rotor in Fig. 11 can be decoupled from variations in the circulation around the rotor in a manner which is not possible with the rotor replaced by a fin, it will be possible to evaluate the pattern of thrust generation reflected in the carangiform wake in comparison to a range of alternatives not seen in nature.

Fig. 12 compares a trajectory described by the device in Fig. 11 to that predicted by a numerical model built upon the lift model (6). The body of the vehicle is assumed to exhibit the effective mass of a cylinder with elliptical cross-section, and to experience a quadratic drag which varies similarly with direction of motion. Oscillations in the position and rotation of the rotor are phased to approximate those corresponding to carangiform swimming following [3] and [41]; the serpentine nature of the trajectories in Fig. 12 ensues accordingly. The agreement between the predicted and observed trajectories further validates the model (6).

We note, finally, that the analogy developed in Section V between the Flettner rotor and a simple mechanical system subject to a nonholonomic constraint implies an analogy between the system in Fig. 11 and systems like the snakeboard [14], [24] and the roller racer [42], which are propelled through the interaction

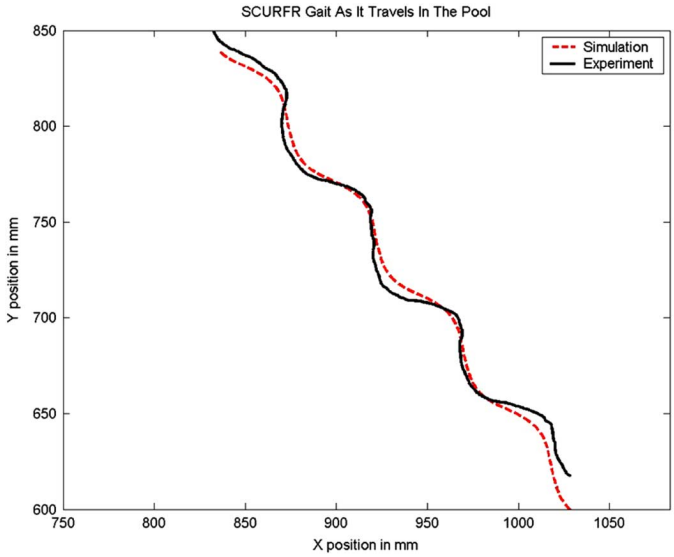

Fig. 12. Predicted and observed trajectories for the robot in Fig. 11.

of constraints and conservation laws. Propulsive oscillations of the rotor in Fig. 11 are particularly evocative of oscillations of the steering arm of the roller racer. We will develop this perspective in a future work.

REFERENCES

[1] L. M. Milne-Thomson, *Theoretical Hydrodynamics*. New York: Dover, 1996.
[2] E. Purcell, "Life at low Reynolds number," *Amer. J. Phys.*, vol. 45, pp. 3–11, 1977.
[3] Sir J. Lighthill, *Mathematical Biofluiddynamics*. Philadelphia, PA: SIAM, 1975.
[4] S. D. Kelly, "The mechanics and control of driftless swimming," *SIAM J. Control Optim.*, submitted for publication.
[5] S. D. Kelly and R. M. Murray, "Geometric phases and robotic locomotion," *J. Robot. Syst.*, vol. 12, pp. 417–431, 1995 [Online]. Available: http://www.cds.caltech.edu/reports (extended version)
[6] R. M. Murray, J. W. Burdick, S. D. Kelly, and J. E. Radford, "Trajectory generation for mechanical systems with application to robotic locomotion," in *Proc. 3rd Int. Workshop Algorithmic Found. Robot.*, 1998.
[7] J. E. Radford and J. W. Burdick, "Local motion planning for nonholonomic mechanical systems evolving on principal bundles," in *Proc. 13th Int. Symp. Math. Theory Netw. Syst.*, 1998.
[8] J. P. Ostrowski, "Optimal control for principal kinematic systems on Lie groups," in *Proc. IFAC World Congr.*, 1999, pp. 539–544.
[9] S. D. Kelly and R. M. Murray, "Modelling efficient pisciform swimming for control," *Int. J. Robust Nonlinear Control*, vol. 10, no. 4, pp. 217–241, 2000.
[10] E. Kanso, J. E. Marsden, C. W. Rowley, and J. Melli-Huber, "Locomotion of articulated bodies in a perfect fluid," *J. Nonlinear Sci.*, vol. 15, pp. 255–289, 2005.
[11] P. T. Tokumaru and P. E. Dimotakis, "The lift of a cylinder executing rotary motions in a uniform flow," *J. Fluid Mech.*, vol. 255, pp. 1–10, 1993.
[12] J. P. Ostrowski, "Steering for a class of dynamic nonholonomic systems," *IEEE Trans. Autom. Control*, vol. 45, no. 8, pp. 1492–1498, Aug. 2000.
[13] J. P. Ostrowski, J. P. Desai, and V. Kumar, "Optimal gait selection for nonholonomic locomotion systems," *Int. J. Robot. Res.*, vol. 19, no. 2, pp. 225–237, 2000.
[14] F. Bullo and A. D. Lewis, "Kinematic controllability and motion planning for the snakeboard," *IEEE Trans. Robot. Autom.*, vol. 19, no. 3, pp. 494–498, Jun. 2003.
[15] K. M. Lynch, "Optimal control of the thrusted skate," *Automatica*, vol. 39, no. 1, pp. 173–176, 2003.

[16] Q. Zhu, M. J. Wolfgang, D. K. P. Yue, and M. S. Triantafyllou, "Three-dimensional flow structures and vorticity control in fish-like swimming," *J. Fluid Mech.*, vol. 468, pp. 1–28, 2002.
[17] J. E. Marsden and T. S. Ratiu, *Introduction to Mechanics and Symmetry*, 2nd ed. New York: Springer-Verlag, 1999.
[18] J. E. Marsden and A. Weinstein, "Coadjoint orbits, vortices, and clebsch variables for incompressible fluids," *Physica 7D*, pp. 305–323, 1983.
[19] P. G. Saffman, *Vortex Dynamics*. Cambridge, U.K.: Cambridge Univ. Press, 1992.
[20] G. A. Tokaty, *A History and Philosophy of Fluid Mechanics*. New York: Dover, 1994.
[21] A. J. Chorin and J. E. Marsden, *A Mathematical Introduction to Fluid Mechanics*, 3rd ed. New York: Springer-Verlag, 1997.
[22] L. M. M. Thomson, *Theoretical Aerodynamics*. New York: Dover, 1973.
[23] D. G. Crighton, "The Kutta condition in unsteady flow," *Annu. Rev. Fluid Mech.*, vol. 17, pp. 411–445, 1985.
[24] A. M. Bloch, P. S. Krishnaprasad, J. E. Marsden, and R. M. Murray, "Nonholonomic mechanical systems with symmetry," *Arch. Rational Mech. Anal.*, vol. 136, pp. 21–99, 1996.
[25] F. Rizzo, "The Flettner rotor ship in the light of the Kutta–Joukowski theory and of experimental results," *Nat. Advisory Committee for Aeronaut. Tech. Note*, 1925.
[26] S. Salter, "Spray turbines to increase rain by enhanced evaporation from the sea," in *Proc. 10th Congr. Int. Maritime Assoc. Mediterranean*, 2002, CD-ROM.
[27] Lord Kelvin, "On vortex motion," *Trans. Roy. Soc. Edinburgh*, vol. 25, pp. 217–260, 1869.
[28] P. K. Newton, *The N-Vortex Problem*. New York: Springer-Verlag, 2001.
[29] B. N. Shashikanth, J. E. Marsden, J. W. Burdick, and S. D. Kelly, "The Hamiltonian structure of a 2-D rigid circular cylinder interacting dynamically with N point vortices," *Phys. Fluids*, vol. 14, pp. 1214–1227, 2002.
[30] C. M. Breder, "The locomotion of fishes," *Zoologica*, vol. 4, pp. 159–297, 1926.
[31] J.-M. Coron, "On the controllability of the 2-D incompressible Navier–Stokes equations with the Navier slip boundary conditions," *ESAIM: Control, Optim. Calculus Var.*, vol. 1, pp. 35–75, 1996.
[32] H. G. Magnus, "Über die Abweichung der Geschesse," *Poggendorf's Annalen der Physik u. Chemie*, vol. 88, pp. 1–14, 1853.
[33] G. Birkhoff, *Hydrodynamics: A Study in Logic, Fact, and Similitude*. Westport, CT: Greenwood, 1978.
[34] H. Nijmeijer and A. J. van der Schaft, *Nonlinear Dynamical Control Systems*. New York: Springer-Verlag, 1996.
[35] M. P. do Carmo, *Differential Geometry of Curves and Surfaces*. Englewood Cliffs, NJ: Prentice-Hall, 1976.
[36] L. E. Dubins, "On curves of minimal length with a constraint on average curvature, and with prescribed initial and terminal positions and tangents," *Amer. J. Math.*, vol. 3, pp. 497–516, 1957.
[37] J. P. Ostrowski, "The mechanics and control of undulatory locomotion," Ph.D. dissertation, California Inst. Technol., Pasadena, CA, 1995.
[38] A. M. Bloch, *Nonholonomic Mechanics and Control*. New York: Springer-Verlag, 2003.
[39] P. Grassberger and I. Procaccia, "Measuring the strangeness of strange attractors," *Physica D*, vol. 9, no. 189, pp. 189–208, 1983.
[40] E. Ott, *Chaos in Dynamical Systems*, 2nd ed. Cambridge, U.K.: Cambridge Univ. Press, 2002.
[41] M. S. Triantafyllou, G. S. Triantafyllou, and D. K. Yue, "Hydrodynamics of fishlike swimming," *Annu. Rev. Fluid Mech.*, vol. 32, pp. 33–53, 2000.
[42] P. S. Krishnaprasad and D. P. Tsakiris, "Oscillations, SE(2)-Snakes and motion control," Univ. Maryland, Center Dyn. Control Smart Struct., College Park, MD, ech. Rep. CDCSS TR 98-4, 1998.

Scott D. Kelly (M'01) received the B.S degree in mechanical and aerospace engineering from Cornell University, Ithaca, NY, in 1991 and the M.S. and Ph.D. degrees in mechanical engineering from the California Institute of Technology, Pasadena, in 1992 and 1998, respectively.

He was a Research Engineer in Biological Systems Modeling with Entelos, Inc., Foster City, CA, from 1999 to 2001. He has been an Assistant Professor in the Department of Mechanical Science and Engineering, University of Illinois at Urbana-Champaign, Urbana, since 2001. His research interests include geometric mechanics, nonlinear dynamics and control, and mathematical biology.

Dr. Kelly received National Science Foundation CAREER and PECASE awards in 2005 and 2006, respectively.

Ramadev B. Hukkeri received the B.S. and M.S. degrees in mechanical engineering from the University of Illinois at Urbana-Champaign, Urbana, in 2002 and 2004, respectively. His studies were focused on robotics.

Since 2004, he has been building a startup company developing novel visual aids and robotic prostheses. He resides in Chicago, IL.